

# A renormalization method for three-boson system with a triboson field

Shung-Ichi Ando\*

*School of Mechanical and ICT Convergence Engineering,  
Sunmoon University, Asan, Chungnam 31460*

(Received 16 December 2016)

## Abstract

A renormalization method that introduces an auxiliary field to represent a three-body bound state is studied in a three-boson system with a triboson field. A cutoff dependence in the three-boson system emerges as a limit cycle, and the cyclic singularity is renormalized by employing two methods: a standard method and the auxiliary field method. For each method, different sets of diagrams are involved for renormalization, and thus we numerically study three quantities: counter term for renormalization, scattering length of  $s$ -wave boson-diboson scattering, and normalized wavefunction. We confirm that the two methods would lead to the same result.

PACS numbers: 11.10.Gh, 21.45.-v

Keywords: Suggested keywords

arXiv:1701.01200v1 [nucl-th] 5 Jan 2017

---

\*Electronic address: sando@sunmoon.ac.kr

## I. INTRODUCTION

The studies of three-body systems in pionless effective field theory (EFT) revealed a nontrivial feature of the systems. That is an appearance of a cyclic singularity, known as a limit cycle, in a three-boson system [1] and a three-nucleon system in triton channel [2]. A three-body contact interaction, whose order is naively counted as that in higher order, is promoted to leading order (LO) for renormalization of the singularity. The appearance of the limit cycle is accompanied by emergence of bound states, known as Efimov states, in the unitary limit [3]. For recent studies of the three-nucleon systems in triton and  ${}^3\text{He}$  channels, one may refer to Refs. [4–7]. (For general reviews of the pionless EFT, one may refer to Refs. [8, 9].) This feature is also applied to the studies of the various systems, e.g., halo-nuclei [10] and hyper-nuclei [11–15].

One of the issues of the three-nucleon systems in pionless EFT is to establish a rigorous perturbative method to expand an amplitude in terms of effective range terms because the major part of the previous works employed an approximation so called partially resummed approach [16]. A fully perturbative method for a calculation of  $nd$  scattering in pionless EFT was suggested by Vanasse. However, it is not easy to apply the method to a study involving a bound state [17]. Recently, the same author suggested a new method to deal with a bound state perturbatively by introducing a tribaryon field, which represents the bound state of triton, and the method was applied to a calculation of charge radius of the triton up to next-to-next-to-leading order [18].

This new method introduces an auxiliary field which represents a bound state of a three-body system. A dressed three-body propagator is constructed by using the auxiliary field, and a coupling constant of the auxiliary field is determined so that a pole position of the three-body binding energy is reproduced in the dressed three-body propagator. An advantage of the new method is that it is not necessary to numerically fit the coupling constant of the three-body part by employing Newton’s method. The method has originally been introduced by Hagen et al., and they applied it to the study of electric form factor of two-neutron halo systems [19].

In this short report, we study the renormalization method suggested by Hagen et al. by employing a simple system, three neutral scalar boson system of equal masses with a triboson field. Using a simple system is beneficial to a study of the renormalization method itself since

it avoids detailed calculations. The system exhibits a limit cycle, thus a sharp momentum cutoff  $\Lambda$  is introduced in an integral equation for the three-boson system, and a value of a three-body coupling is determined as functions of  $\Lambda$  by employing two methods: a standard method and the auxiliary field method. In the two methods, as to be discussed in detail later, sets of diagrams involved in the scattering amplitude are the same. However, those for renormalization and calculations of a normalized wavefunction are different. So it would be worth confirming that the two different methods lead to an identical result. We then numerically calculate scattering length of  $s$ -wave boson-diboson scattering and normalized wavefunctions, and we confirm that the two method would lead to the same result.

This work is organized as following. In Sec. 2, an effective Lagrangian for a three-boson system with a triboson field is displayed, and in Sec. 3, two-body and three-body parts of an equation for the three-body system are constructed from the Lagrangian for the two renormalization methods. In Sec. 4, numerical results are obtained, and finally in Sec. 5, results and discussion of the work are presented.

## II. LAGRANGIAN

To study the renormalization method for a three-body system, we consider a simple system, three neutral scalar bosons having equal masses, which makes a two-body bound state and a three-body bound state. In addition, we employ standard counting rules in pionless EFT for two and three-body systems [2, 8]. Here we consider LO contributions only. Thus we employ a simple Lagrangian for the three-boson system including diboson and triboson fields as [19–23]

$$\begin{aligned}
\mathcal{L} = & \phi^\dagger \left( i\partial_0 + \frac{1}{2m}\nabla^2 \right) \phi + \dots \\
& + d^\dagger \Delta_d d - \frac{1}{2} y_d (d^\dagger \phi \phi + \phi^\dagger \phi^\dagger d) + \dots \\
& + t^\dagger \Delta_t t - y_t (t^\dagger d \phi + d^\dagger \phi^\dagger t) + \dots, \tag{1}
\end{aligned}$$

where  $\phi$ ,  $d$ , and  $t$  are boson, diboson, and triboson fields, respectively, and  $m$  is the boson mass. The dots denote higher order terms which have more derivatives. Four parameters,  $\Delta_d$ ,  $\Delta_t$ ,  $y_d$ , and  $y_t$ , appear in the Lagrangian at LO.  $\Delta_d$  and  $\Delta_t$  are fixed by using two and three-body binding energies,  $B_2$  and  $B_3$ , respectively, whereas  $y_d$  and  $y_t$  can arbitrarily be chosen.

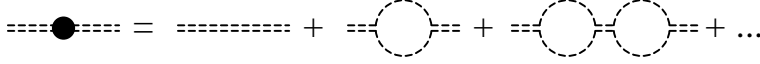


FIG. 1: Diagrams for propagator of dressed diboson field. A double (single) dashed line denotes bare diboson (boson) field.

### III. AMPLITUDES

Two-body and three-body parts of an amplitude for the three-boson system are presented in the following, and we discuss a limit cycle appearing in the three-body part.

#### A. Two-body part

In Fig. 1, diagrams of a dressed diboson propagator are depicted where the two-boson bubble diagrams are summed up to infinite order. One may have the renormalized dressed diboson propagator as [23]

$$D_d(p_0, \vec{p}) = \frac{1}{\gamma_d - \sqrt{-mp_0 + \frac{1}{4}\vec{p}^2} - i\epsilon}, \quad (2)$$

where  $p_0$  and  $\vec{p}$  are off-shell energy and three momentum of the propagation of the diboson state, and parameters in the propagator have been fixed as  $y_d^2 = \frac{8\pi}{m}$ ,  $\gamma_d = \sqrt{mB_2} = \Delta_d$  where  $\gamma_d$  is the binding momentum of the two-boson bound state. The wavefunction normalization factor  $Z_d$  of the diboson field is obtained by using the relation,  $Z_d^{-1} = \left. \frac{dD_d^{-1}(E, \vec{0})}{dE} \right|_{E=-B_2}$ , as

$$Z_d = \frac{2\gamma_d}{m}. \quad (3)$$

#### B. Three-body part

We construct the three-body part in two ways. We refer to a conventional method as “standard renormalization method” (SM) and, to the one suggested by Hagen et al., the “auxiliary field renormalization method” (AM) in the following.

##### 1. Standard renormalization method (SM)

In Fig. 2, diagrams of an integral equation for  $s$ -wave boson-diboson scattering in terms of a scattering amplitude are depicted. Thus one has an integral equation from the diagrams



FIG. 2: Diagrams for integral equation of  $s$ -wave boson-diboson scattering. A shaded blob denotes an elastic scattering amplitude, and a triple dashed line does propagation of a bare triboson field. See the caption of Fig. 1 as well.

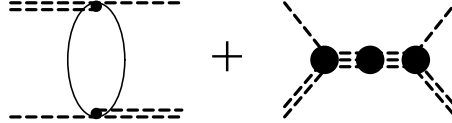


FIG. 3: Diagrams for scattering amplitude for  $s$ -wave diboson-boson scattering.

in Fig. 2 as [1]

$$t(p, k) = \frac{4\pi}{pk} \ln \left( \frac{p^2 + k^2 + pk - mE}{p^2 + k^2 - pk - mE} \right) - \frac{y_t^2}{\Delta_t} - \frac{2}{(2\pi)^2} \int_0^\Lambda dl l^2 \left[ \frac{4\pi}{pl} \ln \left( \frac{p^2 + l^2 + pl - mE}{p^2 + l^2 - pl - mE} \right) - \frac{y_t^2}{\Delta_t} \right] \frac{t(l, k)}{\gamma_d - \sqrt{-mE + \frac{3}{4}l^2}}, \quad (4)$$

where  $t(p, k)$  is the scattering amplitude of  $s$ -wave boson-diboson scattering and  $p$  ( $k$ ) is the magnitude of off-shell (on-shell) relative momentum in final (initial) boson-diboson state in center of mass frame. A sharp cutoff  $\Lambda$  is introduced for renormalization in the equation. For the renormalization using the three-body binding energy, the homogeneous part of the integral equation in Eq. (4) is numerically solved by choosing  $E = -B_3$ , and the parameter  $y_t^2/\Delta_t$  is fitted as a function of  $\Lambda$ . The numerical method to solve the equation is described in Ref. [4].

## 2. Auxiliary field renormalization method (AM)

For the auxiliary field renormalization method (AM), Feynman diagrams of the on-shell scattering amplitude  $t(k, k)$  are depicted in Fig. 3. The scattering amplitude  $t(k, k)$  is represented as [18, 19]

$$t(k, k) = a(k, k) + b(k, k), \quad (5)$$

where  $a(k, k)$  is a scattering amplitude without including the triboson field. In Fig. 4, diagrams of the scattering amplitude  $a(k, k)$  are depicted, and  $a(k, k)$  is calculated by solving



FIG. 4: Diagrams for integral equation of scattering amplitude without triboson propagator. See the caption of Fig. 1 as well.

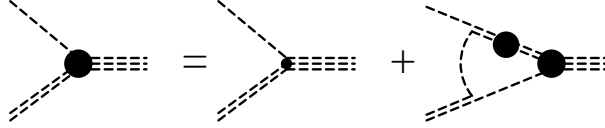


FIG. 5: Diagrams for integral equation of three-point boson-diboson-triboson vertex. A three-point vertex with a filled circle (a dot) denotes a dressed (bare) vertex. See the caption of Fig. 1 as well.

the integral equation in Eq. (4) without including the triboson field. On the other hand,  $b(k, k)$  is a scattering amplitude through the propagation of a dressed triboson field,

$$b(k, k) = -Y_t(k, E)D_t(E)Y_t(k, E), \quad (6)$$

where  $Y_t(k, E)$  is a dressed boson-diboson-triboson vertex function, and  $D_t(E)$  is a dressed triboson propagator. In Fig. 5, diagrams of the dressed boson-diboson-triboson vertex  $Y_t(p; E)$  are depicted. Thus one has an integral equation for  $Y_t(p; E)$  as

$$Y_t(p, E) = y_t - \frac{2}{\pi} \int_0^\Lambda dl l^2 \frac{1}{pl} \ln \left( \frac{p^2 + l^2 + pl - mE}{p^2 + l^2 - pl - mE} \right) \frac{Y_t(l, E)}{\gamma_d - \sqrt{-mE + \frac{3}{4}l^2}}. \quad (7)$$

In Fig. 6, diagrams for the dressed triboson propagator, which is obtained by summing a self-energy term up to infinite order, are depicted. Thus, from the diagrams, one has the dressed triboson propagator as

$$D_t(E) = \frac{1}{\Delta_t - \Sigma_t(E)}, \quad (8)$$

where  $\Sigma_t(E)$  is the self-energy term whose diagrams are depicted in Fig. 7. Thus we have

$$\Sigma_t(E) = \frac{y_t}{2\pi^2} \int_0^\Lambda dl \frac{l^2 Y_t(l, E)}{\gamma_d - \sqrt{-mE + \frac{3}{4}l^2}}. \quad (9)$$

The parameter  $\Delta_t$  is fixed so as to reproduce the pole structure of the three-body binding energy at  $E = -B_3$  in the dressed triboson propagator. We note that the diagrams involving

$$\text{triple dashed line with filled circle} = \text{triple dashed line} + \text{triple dashed line with filled square} + \text{triple dashed line with two filled squares} + \dots$$

FIG. 6: Diagrams for dressed triboson propagator. A triple dashed line denotes a bare triboson propagation and a filled box does a self-energy term obtained in Fig. 7.

$$\text{triple dashed line with filled square} = \text{triple dashed line} \text{ connected to a loop of two dashed lines with filled circles}$$

FIG. 7: Diagrams for self-energy of the triboson propagation. See the captions of Figs. 1 and 5 as well.

in the scattering state in Figs. 2 and 3 for SM and AM, respectively, are the same, whereas those for renormalization using the three-body binding energy are different. For example, an infinite loop diagram due to one-boson-exchange interaction is included for renormalization in SM, whereas this term exists in the amplitude  $a(k, k)$  and is excluded for renormalization in AM.

### C. Limit cycle of the integral equations

The integral equations for  $t(p, k)$ ,  $a(p, k)$ , and  $Y_t(p, E)$  become the same in asymptotic limit where  $\Lambda \rightarrow \infty$ ,  $p, l \gg E, \gamma_d, k$ , and thus one has, e.g., for  $t(p, k)$  as [1, 12]

$$t(p) = \frac{4}{\sqrt{3}\pi} \int_0^\infty \frac{dl}{p} \ln \left( \frac{p^2 + l^2 + pl}{p^2 + l^2 - pl} \right) t(l), \quad (10)$$

where the  $k$  dependence in  $t(p, k)$  is dismissed above. Then the integral equation becomes scale free, and that indicates a power behavior of the amplitudes in the asymptotic limit,

$$t(p, k), a(p, k), Y_t(p, E) \propto p^{s-1}. \quad (11)$$

After performing a Mellin transformation in Eq. (10) using the relation in Eq. (11), one has [1, 24, 25]

$$1 = \frac{8}{\sqrt{3}s} \frac{\sin\left(\frac{1}{6}\pi s\right)}{\cos\left(\frac{1}{2}\pi s\right)}. \quad (12)$$

The solution of  $s$  for the equation becomes imaginary,  $s = \pm i s_0$  and  $s_0 = 1.0064\dots$ . The imaginary solution indicates the emergence of a limit cycle. The limit cycle exhibiting in  $t(p, k)$  is renormalized by the three-body counter term in SM, whereas those in  $a(p, k)$  and

$Y_t(p, E)$  (as well as  $\Sigma_t(E)$ ) are not in AM. They will be sensitive to a value of the cutoff  $\Lambda$ , and bound states emerge as Efimov states in them.

Apart from the diagrams involving in the renormalization are different in the two methods, when the dressed three-body propagator  $D_t(E)$  is renormalized in AM so as to reproduce the three-body binding pole in it, other bound states can emerge as Efimov states in the other parts,  $a(k, k)$  and  $Y_t(k, E)$ , in the amplitude  $t(k, k)$ . In addition, when a normalized wavefunction is derived in AM, the wavefunction is obtained from the amplitude  $b(k, k)$ , and the amplitude  $a(k, k)$  is excluded from the derivation of the wavefunction even though bound states are generated in it. Those observations are the main concern in the present work, and we are going to numerically study them in the next section.

#### IV. NUMERICAL RESULTS

The three-boson system we study in the present work may not have a corresponding real physical system. Thus, for numerical study of the renormalization method in the three-boson system, we employ values of mass, two and three-body binding energies of the three-nucleon system in triton channel:

$$m = 940 \text{ MeV}, \quad B_2 = 2.22 \text{ MeV}, \quad B_3 = 8.48 \text{ MeV}, \quad (13)$$

and the binding momentum  $\gamma_d$  for the diboson system is  $\gamma_d = \sqrt{mB_2} \simeq 45.7 \text{ MeV}$ .

##### A. Renormalization at three-body binding energy

The integral equations in Eqs. (4) and (7) exhibit a limit cycle, and we renormalize the cyclic singularity at the three-body binding energy,  $E = -B_3$ , with a given value of the cutoff  $\Lambda$  by employing the two methods, SM and AM.

For the standard renormalization method, SM, we solve the homogeneous part of the integral equation in Eq. (4) employing a standard expression of the counter term as [1]

$$\frac{H(\Lambda)}{\Lambda^2} = -\frac{y_t^2}{8\pi\Delta_t}. \quad (14)$$

For the auxiliary field renormalization method, AM, on the other hand, the coupling constant  $\Delta_t$  is determined by using the pole position of three-body bound state in the dressed triboson



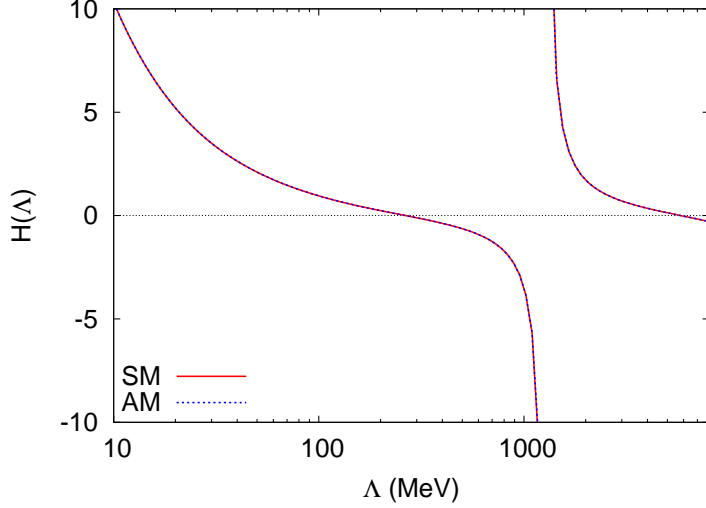


FIG. 8:  $H(\Lambda)$  as functions of cutoff  $\Lambda$  for SM and AM.

propagator in Eq. (8) as [19]

$$\Delta_t - \Sigma_t(-B_3) = 0. \quad (15)$$

Using Eq. (14) we have

$$H(\Lambda) = -\frac{\Lambda^2}{8\pi} \frac{y_t^2}{\Sigma_t(-B_3)}, \quad (16)$$

for AM. We note that  $H(\Lambda)$  for AM does not depend on  $y_t^2$  because of  $\Sigma_t(-B_3) \propto y_t^2$ . In addition, as mentioned above, the diagrams for renormalization involving in SM and AM are different. In SM, one has  $2^n$   $n$ -loop diagrams with  $n \rightarrow \infty$  from the homogeneous part of the integral equation in Eq. (4), and a value of  $H(\Lambda)$  is numerically searched by using Newton's method at the point where the determinant of the matrix vanishes with  $E = -B_3$ . In AM, on the other hand, one has all possible bubble diagrams in the self-energy term,  $\Sigma_t(E)$  in Eq. (9), and a value of  $H(\Lambda)$  is calculated using Eq. (16).

In Fig. 8, we plot curves of  $H(\Lambda)$  as functions of  $\Lambda$  for SM and AM. For the both methods, SM and AM, we reproduce a cyclic pattern in the counter term  $H(\Lambda)$  representing a limit cycle for the three-boson system. In addition, even though the diagrams involving in the two renormalization methods are different, we obtained the same curves of  $H(\Lambda)$  for SM and AM.

In Fig. 9, we plot curves of first and second binding energies,  $B_3^{(1)}$  and  $B_3^{(2)}$ , which appear due to the limit cycle in the amplitudes  $t$  and  $a$  and the dressed vertex function

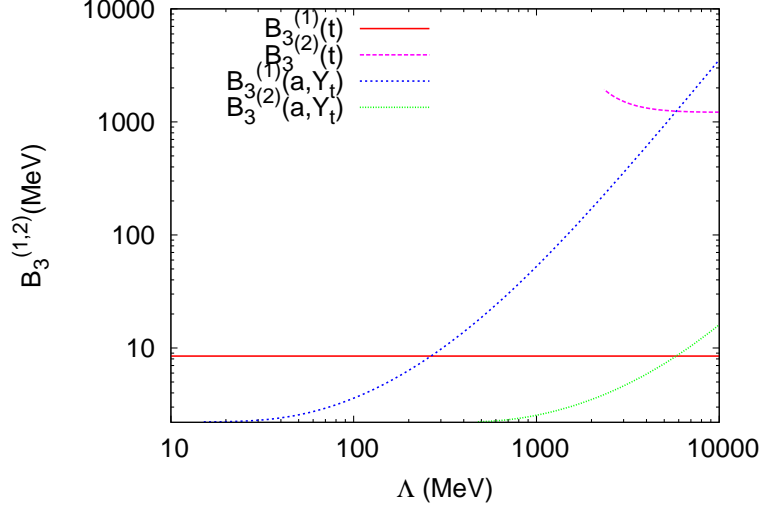


FIG. 9: First and second binding energies  $B_3^{(1)}$  and  $B_3^{(2)}$  appearing in amplitudes  $t$  and  $a$  and dressed vertex function  $Y_t$  as functions of  $\Lambda$ . See the text for details.

$Y_t$ , as functions of  $\Lambda$ . Because the first binding energy  $B_3^{(1)}$  appearing in the amplitude  $t$  is used as input for renormalization in SM, we have a horizontal line which corresponds to  $B_3^{(1)} = B_3 = 8.48$  MeV. A curve of second binding energy,  $B_3^{(2)} \sim 1.2$  GeV, in the amplitude  $t$  appears almost flat and starts around  $\Lambda \simeq 1300$  MeV. One can expect that such a deep binding energy will not affect physics at low energies. Meanwhile, one may be concerned that the system can decay into the deeply bound state once it is formed. Thus one may choose an upper limit of the cutoff value less than  $\Lambda \simeq 1.3$  GeV for the present system.

In AM, the position of the binding energy  $B_3$  is reproduced in the propagator  $D_t(E)$  due to the renormalization, whereas bound states are created in the other parts,  $a$  and  $Y_t$ , of the amplitude  $t(k, k)$  due to the limit cycle. First binding energy  $B_3^{(1)}$  in  $a$  and  $Y_t$  starts appearing around  $\Lambda \simeq 15$  MeV. The binding energy  $B_3^{(1)}$  at the starting point is just above the two-body binding energy,  $B_3^{(1)} \simeq B_2 = 2.22$  MeV, and it increases as the cutoff value increases. Second binding energy  $B_3^{(2)}$  in  $a$  and  $Y_t$  starts appearing around  $\Lambda \simeq 480$  MeV and similarly behaves to the first binding energy  $B_3^{(1)}$ . At the point where the second binding energy appears the first binding energy  $B_3^{(1)}$  becomes  $B_3^{(1)} \simeq 17.6$  MeV. Thus  $a$  and  $Y_t$  contain the small binding energies at the wide range of the cutoff value,  $\Lambda = 15$ -10000 MeV in the figure, and one may expect that those quantities are quite sensitive to the cutoff  $\Lambda$ .

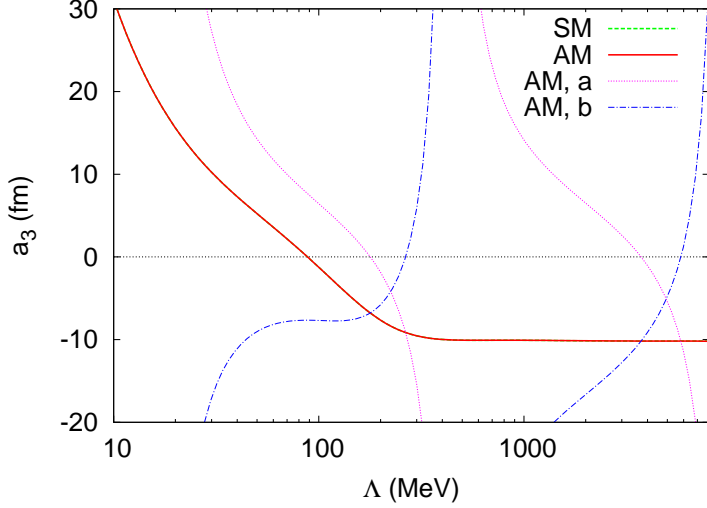


FIG. 10: Scattering length  $a_3$  (fm) for  $s$ -wave diboson-boson scattering as functions of cutoff  $\Lambda$  (MeV) for each of renormalization schemes, SM and AM. Curves of each contribution from  $a(k, k)$  and  $b(k, k)$  amplitudes in Eq. (5) for AM are also plotted.

### B. Scattering length of $s$ -wave boson-diboson scattering

Scattering length  $a_3$  of  $s$ -wave boson-diboson scattering is calculated by using a formula [26],

$$a_3 = -\frac{m}{3\pi}T(0), \quad (17)$$

where the scattering matrix  $T(E)$  is given as  $T(E) = Z_d t(k, k)$ , with  $E = \frac{3}{4m}k^2 - B_2$ , and the wavefunction normalization factor  $Z_d$  of the diboson field has been presented in Eq. (3). The on-shell amplitude  $t(k, k)$  is calculated by solving the integral equation in Eq. (4) for SM, and that is given in Eq. (5) for AM.

In Fig. 10, curves of the scattering length  $a_3$  for the renormalization methods SM and AM are plotted as functions of the cutoff  $\Lambda$ . Curves of  $a_3$  from each component of the amplitudes  $a(k, k)$  and  $b(k, k)$  in Eq. (5) for AM are also included in the figure. We find the same curve of  $a_3$  for SM and AM. It is natural because the diagrams of the scattering amplitude as well as the values of  $H(\Lambda)$  are the same for SM and AM. As seen in the figure, at small cutoff values  $a_3$  are positive. As the value of the cutoff  $\Lambda$  increases, the value of  $a_3$  decreases. And when the value of  $\Lambda$  becomes larger than about  $\Lambda = 300$  MeV,  $a_3$  converges to  $a_3 \simeq -10$  fm. The behavior of  $a_3$  at the small cutoff values implies an artificial effect that an important

part of the momentum flow in the loops is missing at such small cutoff values [26]. For AM, a contribution from each of the components  $a(k, k)$  and  $b(k, k)$  in Eq. (5), as discussed in the previous subsection, is sensitive to the cutoff  $\Lambda$  and exhibits the limit cycle. But after they are added together, one can obtain the cutoff-independent result at  $\Lambda > 300$  MeV.

### C. Normalized wavefunctions

In SM, a wavefunction for relative boson-diboson part of the three-boson bound state is calculated by solving the homogeneous part of the integral equation in Eq. (4). Because the kernel of the integral equation depends on the energy, a normalization condition of the wavefunction becomes nontrivial [27]. For a wavefunction  $|\Psi\rangle$ , which satisfies an equation  $|\Psi\rangle = DK|\Psi\rangle$ , one has a normalization condition of the wavefunction as [5]

$$\langle\psi|D\frac{d}{dE}(D^{-1}-K)D|\psi\rangle=1, \quad (18)$$

where  $|\Psi\rangle = D|\psi\rangle$ . In our case, the operators  $D$  and  $K$  are realized as  $D \rightarrow D_d$  in Eq. (2), and

$$K \rightarrow K(p, l; E) = \frac{4\pi}{pl} \ln \left( \frac{p^2 + l^2 + pl - mE}{p^2 + l^2 - pl - mE} \right), \quad (19)$$

and thus we have a normalization condition of the wavefunction as

$$\begin{aligned} & \frac{m}{4\pi^2} \int_0^\Lambda dl l^2 \left( \frac{\phi_S(l)}{\gamma_d - \sqrt{mB_3 + \frac{3}{4}l^2}} \right)^2 \frac{1}{\sqrt{mB_3 + \frac{3}{4}l^2}} \\ & - \frac{2m}{\pi^3} \int_0^\Lambda dl' l'^2 \int_0^\Lambda dl l^2 \frac{\phi_S(l')}{\gamma_d - \sqrt{mB_3 + \frac{3}{4}l'^2}} \frac{1}{(l'^2 + l^2 + mB_3)^2 - l'^2 l^2} \frac{\phi_S(l)}{\gamma_d - \sqrt{mB_3 + \frac{3}{4}l^2}} \\ & = 1, \end{aligned} \quad (20)$$

where  $\phi_S(p) = t(p, k)|_{E=-B_3}$  is a wavefunction of the bound state obtained in SM.

A normalized wavefunction  $\phi_A$  is obtained from the dressed vertex function  $Y_t(p, E)$  for AM as [19]

$$\phi_A(p) = -\sqrt{Z_t} Y_t(p, -B_3), \quad (21)$$

where we have included an overall minus sign in the expression above so as to obtain a positive value of the wavefunction at  $p = 0$ .  $Z_t$  is the wavefunction normalization factor of

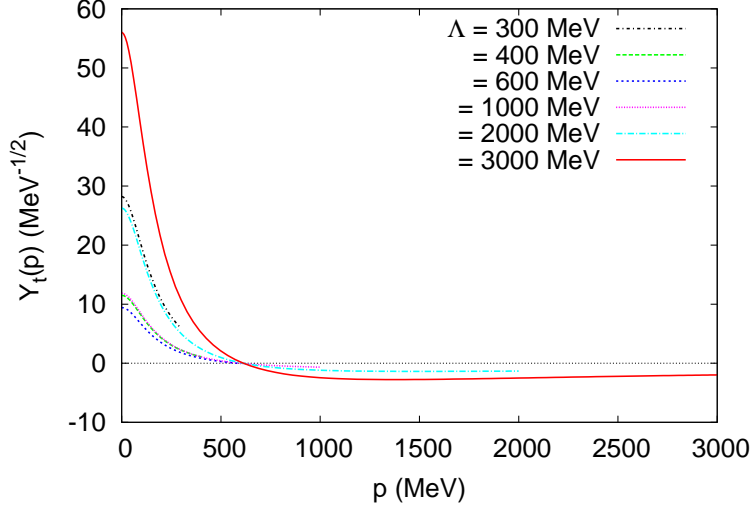


FIG. 11: Dressed vertex function  $Y_t(p, -B_3)$  as functions of  $p$  with various cutoff values  $\Lambda = 300$  to 3000 MeV in AM with  $y_t = 1 \text{ MeV}^{-1/2}$ .

the dressed triboson field and is obtained from the propagator  $D_t(E)$  in Eq. (8). Thus one has

$$Z_t = -\frac{1}{\Sigma'_t(-B_3)}, \quad (22)$$

where  $\Sigma'_t(E) = \frac{d}{dE}\Sigma_t(E)$ . We note that the wavefunction  $\phi_A$  does not depend on  $\Delta_t$ , which is used for normalization in Eq. (15). In addition,  $\phi_A$  does not depend on  $y_t$  either because the coupling  $y_t$  is cancelled between those in the vertex  $Y_t(p, E)$  and the normalization factor  $\sqrt{Z_t}$ . Thus one cannot make the wavefunction  $\phi_A(p)$  cutoff independence by adjusting the parameters,  $y_t$  and  $\Delta_t$ . Furthermore, a part of the amplitude,  $a(k, k)$ , which exhibits a limit cycle and generates bound states in it, is not included in the calculation of  $\phi_A(p)$ . It might be interesting to examine if the wavefunction  $\phi_A$  can be cutoff-independence (in other words, if the limit cycle in  $Y_t(p, -B_3)$  can be cancelled with that in the wavefunction normalization factor  $\sqrt{Z_t}$ ) along with whether  $\phi_A(p)$  is the identical to  $\phi_S(p)$  or not.

In Figs. 11 and 12, we plot curves of the dressed vertex function  $Y_t(p, -B_3)$  and those of normalized wavefunctions  $\phi_A(p)$ , respectively, as functions of relative momentum  $p$  using various cutoff values from 300 to 3000 MeV for AM where we have used  $y_t = 1 \text{ MeV}^{-1/2}$  for  $Y_t(p, -B_3)$ . As seen in Fig. 11, overall factors of the curves of  $Y_t(p, -B_3)$  show a cutoff-dependence, whereas one can see in Fig. 12 that the cutoff dependence in the overall factor of  $Y_t(p, -B_3)$  disappears in the normalized wavefunction  $\phi_A(p)$ . On the other hand,

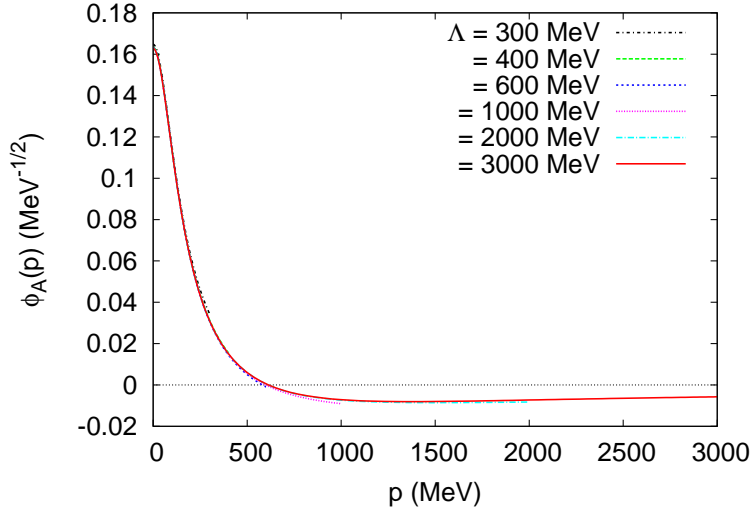


FIG. 12: Normalized wavefunction  $\phi_A(p)$  as functions of  $p$  with various cutoff values  $\Lambda = 300$  to 3000 MeV for AM.

the normalized wavefunction for SM,  $\phi_S(p)$ , is indeed cutoff-independent because of the renormalization. We find the same  $p$ -dependence of the normalized wavefunctions for SM and AM and a difference in the overall factors between them (we do not show a figure for  $\phi_S(p)$ ). The factor difference is about 2.36, and we have  $\phi_S(p) \simeq 2.36 \phi_A(p)$ .

## V. DISCUSSION AND CONCLUSIONS

In the present work, we have studied the auxiliary field renormalization method suggested by Hagen et al. employing a three-boson system with a triboson field. We numerically calculated the coupling of the three-body contact interaction for renormalization, the scattering length  $a_3$  of  $s$ -wave boson-diboson scattering, and the normalized wavefunctions as functions of the cutoff  $\Lambda$  employing the two renormalization methods, SM and AM. We confirm that the three-body system exhibits a limit cycle, and the cyclic singularity can be renormalized by using the both methods. Though the different diagrams are involved for renormalization in those two methods, we obtained the identical result for the renormalized coupling constant of the three-body contact interaction as well as the scattering length  $a_3$ . In addition, we find that the normalized wavefunctions turned out to be cutoff independent, however, we obtained the different overall factors of the normalized wavefunctions in the two methods.

It may be interesting to point out that even though the detailed diagrams involving in

the two renormalization methods and the calculation methods are different, the results of the renormalization of the coupling constants turned out to be the same. Thus, because the diagrams for the scattering amplitude and the renormalized coupling  $H(\Lambda)$  are the same for SM and AM, it is natural to obtain the same scattering length  $a_3$ , in which the limit cycle is renormalized, for the both methods. On the other hand, the parts of the scattering lengths  $a_3$ ,  $a(0,0)$  and  $b(0,0)$ , for AM are indeed sensitive to the cutoff and exhibit the limit cycle.

For the normalized wavefunction  $\phi_A(p)$ , it is also interesting to point out that it is not necessary to renormalize and fix the parameter  $\Delta_t$  in the dressed triboson propagator  $D_t(E)$ . As mentioned above, the two normalized wavefunctions,  $\phi_S(p)$  and  $\phi_A(p)$ , are obtained from the different diagrams and the different calculation methods, while  $\phi_S(p)$  and  $\phi_A(p)$  turned out to be the same function of  $p$  except for the overall factors. Nevertheless, one would have a same result of a physical observable, e.g., electric form factor, in the both renormalization methods after normalizing the wavefunctions by using an available conservative quantity such as a baryon number or an electric charge.

### Acknowledgments

The author would like to thank M. Birse and J. Vanasse for discussion and communications. This work was supported by the Basic Science Research Program through the National Research Foundation of Korea funded by the Ministry of Education of Korea (Grant No. NRF-2016R1D1A1B03930122) and in part by the National Research Foundation of Korea (NRF) grant funded by the Korean government (Grant No. NRF-2016K1A3A7A09005580).

- 
- [1] P.F. Bedaque, H.-W. Hammer, U. van Kolck, Nucl. Phys. **A** 646, 444 (1999).
  - [2] P.F. Bedaque, H.-W. Hammer, U. van Kolck, Nucl. Phys. **A** 676, 357 (2000).
  - [3] V.N. Efimov, Yad. Fiz. **12**, 1080 (1970) [Sov. J. Nucl. Phys. **12**, 589 (1971)].
  - [4] S.-I. Ando and M.C. Birse, J. Phys. G **37**, 105108 (2010).
  - [5] S. König and H.-W. Hammer, Phys. Rev. C **83**, 064001 (2011).
  - [6] J. Vanasse *et al.*, Phys. Rev. C **89**, 064003 (2014).
  - [7] S. König *et al.*, J. Phys. G **43**, 055106 (2016).
  - [8] P.F. Bedaque and U. van Kolck, Annu. Rev. Nucl. Part. Sci. **52**, 339 (2002).

- [9] E. Braaten and H.-W. Hammer, Phys. Rep. **428**, 259 (2006).
- [10] See, e.g., H.-W. Hammer, EPJ Web of Conf. **113**, 01004 (2016), and references therein.
- [11] H.-W. Hammer, Nucl. Phys. A **22**, 173 (2002).
- [12] S.-I. Ando, Int. J. Mod. Phys. E **25**, 1641005 (2016).
- [13] S.-I. Ando, G.S. Yang, and Y. Oh, Phys. Rev. C **89**, 014318 (2014).
- [14] S.-I. Ando and Y. Oh, Phys. Rev. C **90**, 037301 (2014).
- [15] S.-I. Ando, U. Raha, and Y. Oh, Phys. Rev. C **92**, 024325 (2015).
- [16] F. Gabbiani, P.F. Bedaque, and H.W. Griesshammer, Nucl. Phys. A **675**, 601 (2000).
- [17] J. Vanasse, Phys. Rev. C **88**, 044001 (2013).
- [18] J. Vanasse, arXiv:1512.03805v2 [nucl-th].
- [19] P. Hagen, H.-W. Hammer, and L. Platter, Eur. Phys. J. A **49**, 118 (2013).
- [20] P.F. Bedaque *et al.*, Nucl. Phys. A **714**, 589 (2003).
- [21] H.W. Griesshammer, Nucl. Phys. A **744**, 192 (2004).
- [22] S.R. Beane and M.J. Savage, Nucl. Phys. A **694**, 511 (2001).
- [23] S. Ando and C.-H. Hyun, Phys. Rev. C **72**, 014008 (2005).
- [24] C. Ji, Ph.D. thesis, Ohio University, 2012 (unpublished).
- [25] C. Ji and D.R. Phillips, Few Body Syst. **54**, 2317 (2013).
- [26] S.-I. Ando, Few-Body Syst. **55**, 191 (2014).
- [27] D. Lurie, A.J. Macfarlane, and Y. Takahashi, Phys. Rev. **140**, B1091 (1965).